Volatile Compounds Detection by IR Acousto-optic Detectors

A. D'Amico[12], C. Di Natale[12], F. Lo Castro[1], S. Iarossi[1] and A. Catini[2]

[1] C.N.R. Institute of Acoustics (IDAC), Via del Fosso del Cavaliere 100, 00133 Rome, Italy
[2] University of Rome "Tor Vergata", Dept. of Electronic Engineering, Via del Politecnico 1, 00133 Rome, Italy

Summary. Many important gasses and liquids, including the aggressive or anomalous ones for which our attention is higher, have strong absorption lines in the near and mid infrared spectral range. Infrared sensors exploit the fact that most gasses and liquids present unique infrared signatures in the $2 - 14\mu m$ wavelength region. Due to this uniqueness infrared sensors provide conclusive identification and measurement of the target sample with little interference from other unwanted volatile compounds. Infrared sensors have the characteristics of being highly accurate, reliable, and, in general, low noise devices. In this chapter we will consider the most important infrared sources and sensors as well as the absorption techniques employed in this context. Furthermore the acousto-optic principle will be presented and discussed in some detail as the promoter of a multi-wavelength infrared generator. Finally system performance and data on gas detection will also be introduced and commented upon.

Key words: Infrared spectra: near, medium, far infrared intervals, infrared sources, infrared detectors, acousto-optic devices, volatile compounds infrared absorption.

1 Optical radiation

The International Commission on Illumination (CIE) recommended the division of optical radiation into the following three bands: [14, 15].

- IR-A: $700nm - 1400nm$
- IR-B: $1400nm - 3000nm$
- IR-C: $3000nm - 1mm$

A commonly used sub-division scheme is:

- Near-infrared (NIR, IR-A DIN): $0.75 - 1.4\mu m$ in wavelength, defined by the water absorption, and commonly used in fiber optic telecommunication

because of low attenuation losses in the SiO_2 glass (silica) medium. Image intensifiers are sensitive to this area of the spectrum. Examples include night vision devices such as night vision goggles.
- Short-wavelength infrared (SWIR, IR-B DIN): $1.4 - 3\mu m$, water absorption increases significantly at $1450nm$. The 1530 to 1560 nm range is the dominant spectral region for long-distance telecommunications.
- Mid-wavelength infrared (MWIR, IR-C DIN) also called intermediate infrared (IIR): $3 - 8\mu m$. In guided missile technology the $3 - 5\mu m$ portion of this band is the atmospheric window in which the homing heads of passive IR "heat seeking" missiles are designed to work, homing on to the IR signature of the target aircraft, typically the jet engine exhaust plume.
- Long-wavelength infrared (LWIR, IR-C DIN): $8 - 15\mu m$. This is the "thermal imaging" region, in which sensors can obtain a completely passive picture of the outside world based on thermal emissions only and requiring no external light or thermal source such as the sun, moon or infrared illuminator. Forward-looking infrared (FLIR) systems use this area of the spectrum. Sometimes also called the "far infrared".
- Far infrared (FIR): $15 - 1000\mu m$.

NIR and SWIR is sometimes called reflected infrared while MWIR and LWIR is sometimes referred to as thermal infrared. Due to the nature of the blackbody radiation curves, typical "hot" objects, such as exhaust pipes, often appear brighter in the MW compared to the same object viewed in the LW.

Another scheme is based on the response of various sensors [30]:

- Near Infrared (NIR): from 0.7 to 1.0 μm (from the approximate end of the response of the human eye to that of silicon).
- Short-Wave Infrared (SWIR): from 1.0 to 3 μm (from the cut off of silicon to that of the MWIR atmospheric window. $InGaAs$ covers to about 1.8 micrometers; the less sensitive lead salts cover this region.
- Mid-Wave Infrared (MWIR): from 3 to 5 μm (defined by the atmospheric window and covered by Indium antimonide [$InSb$] and $HgCdTe$ and partially by lead selenide [$PbSe$]).
- Long-Wave Infrared (LWIR): from 8 to 12, or from 7 to 14 μm: the atmospheric window (Covered by $HgCdTe$ and microbolometers).
- Very-Long Wave Infrared (VLWIR): from 12 to about 30 μm, covered by doped silicon.

These divisions are justified by the different human responses to this radiation: near infrared is the region closest in wavelength to the radiation detectable by the human eye, mid and far infrared are progressively further from the visible regime. Other definitions follow different physical mechanisms (emission peaks, vs. bands, water absorption) and the newest follow technical reasons (The common silicon sensors are sensitive to about 1050 nm, while $InGaAs$ sensitivity starts around 950 nm and ends between 1700 and 2600 nm, depending on the specific configuration). Unfortunately, international standards for these specifications are not currently available. The boundary between visible and infrared light is not precisely defined. The human eye is markedly less sensitive to light above 700 nm wavelength, so shorter frequencies make insignificant contributions to scenes illuminated by common light sources. But particularly intense light (e.g., from lasers, or from bright daylight with the visible light removed by colored gels) can be detected up to approximately 780 nm, and will be perceived as red light. The onset of infrared is defined (according to different standards) at various values typically between 700 nm and 800 nm.

2 Infrared sources

2.1 Thermal infrared sources

Thermal sources are resistors of various sorts heated by applying an electric current. Some can be electrically modulated by interrupting the current flow. Others have a larger thermal mass and cannot be modulated effectively at a frequency suitable for most analytical instruments. Black Bodies (B.B.) usually belong to both categories. In fact for many years it has been possible to design and fabricate small B.B. made by thin wires heated at high temperature while, after the advent of micromachining engineering, integrated B.B. have been fabricated and successfully tested. Traditional B.B. have the possibility to deliver high power that can offer modulated B.B. energy through external choppers able to operate mechanically up to a frequency of $5kHz$. Electro-optical choppers can allow an even higher frequency to be reached for particular applications. A B.B. can be considered as a passive structure able to adsorb any radiation frequency and emit a radiation spectra related to its average temperature. Its radiant emittance, or radiance, can be expressed as $R = \epsilon\sigma T$, where ϵ is the emissivity, σ is the Stefan-Boltzman constant equal to: $\sigma = 5.67 \cdot 10^{-8}\ W/(m^2 \cdot K^4)$ and T is the absolute temperature value.

2.2 IR Light Emitting Diodes (LEDs)

2.2.1 Tunable laser diodes

Laser diodes generate light by a single photon being emitted when a high energy electron in the conduction band recombines with a hole in the valence band. The energy of the photon and hence the emission wavelength of laser diodes is therefore determined by the band gap of the material system used. Different diode lasers are available for specific applications in the range over which tuning is to be performed. These lasers can be also tuned by either adjusting their temperature or by changing injection current density into the gain medium. While temperature changes allow tuning over $100cm^{-1}$, it is limited by slow tuning rates (a few hertz), due to the thermal inertia of the system. On the other hand, adjusting the injection current can provide tuning at rates as high as $\sim 10GHz$, but it is restricted to a smaller range (about 1 to 2 cm^{-1}) over which the tuning can be performed. The typical laser linewidth is on the order of $10^{-3}cm^{-1}$ or smaller.

2.2.2 Quantum Cascade Lasers

Quantum cascade lasers (QCLs) are semiconductor lasers that emit in the mid- to far-infrared portion of the electromagnetic spectrum. A QCL however does not use bulk semiconductor materials in its optically active region. Instead it comprises a periodic series of thin layers of varying material composition forming a so called superlattice. The superlattice introduces a varying electric potential across the length of the device, meaning that there is a varying probability of electrons occupying different positions over the length of the device. This is referred to as one-dimensional multiple quantum well confinement and leads to the splitting of the band of permitted energies into a number of discrete electronic subbands. By a suitable design of the layer thicknesses it is possible to engineer a population inversion between two subbands in the system which is required in order to achieve laser emission. Since the position of the energy levels in the system is primarily determined by the layer thicknesses and not by the material, it is possible to tune the emission wavelength of QCLs over a wide range in the same material system. In quantum cascade structures, electrons undergo intersubband transitions and photons are emitted. The electrons tunnel to the next period of the structure and the process repeats. Additionally, in semiconductor laser diodes, electrons and holes are annihilated after recombining across the band gap and can play no further part in photon generation. However in a unipolar QCL, once an electron has undergone an intersubband transition and has emitted a photon in one period of the superlattice, it can tunnel into the next period of the structure where another photon can be emitted. This process of a single electron causing the emission of multiple photons as it goes through the QCL structure gives rise to the name *cascade* and yields a quantum efficiency greater than unity, which leads to higher output powers than semiconductor laser diodes.

3 Sensor types and related materials

3.1 Detection Mechanisms

The most important types of infrared sensors can be classified on the basis of their intrinsic working mechanisms as illustrated below [25].

3.1.1 Quantum sensors

They can be divided in three categories:

a) Photon sensors

a.1 Photoconductive(intrinsic) $Hg_{(1-x)}\,Cd_xTe$, $Pb_{(1-x)}Sn_xTe$, $Pb_{(1-x)}Sn_xSe$. For each x-value a different cut-off frequency is obtained.
a.2 Photoconductive(extrinsic) Ge, $Ge-Si$, $InSb$, $GaAs$ are the most interesting materials. Germanium can be doped by different materials and the following performances can be obtained as far as the cut-off frequency is concerned. $Ge:Au(9\mu m)$, $Ge:Hg(14\mu m)$; $Ge:Cd(23\mu m)$; $Ge:In(105\mu m)$; $Ge:Sb(125\mu m)$. *Types of photoconductivity:*
a.3 Photovoltaic (photodiodes).
a.4 Superconducting sensors (based on the Josephson effect).

b) Thermal sensors (operating at room temperature)

b.1 Golay cell
b.2 Thermistor bolometer
b.3 Thermocouple
b.4 Thermopile
b.5 Pyroelectric

c) Thermal sensors (operating at cryogenic temperature)

c.1 Carbon bolometer
c.2 Ge bolometer
c.3 Si bolometer
c.4 $InSb$ free carrier-absorption bolometer
c.5 Superconducting bolometer

Another kind of classification concerns the presence or not of an external power supply during the signal detection procedure. In this context we have:

1) Active sensors which are those not requiring any external supply, such as

1.a Photovoltaic
1.b Thermocouple and thermopiles
1.c Pyroelectric

2) Passive sensors requiring external DC bias

2.a Photoconductive
2.b All kind of bolometers

3.2 Photon sensors

Photon sensors are based on the absorption of long-wavelength radiation as a result of a specific quantum event, such as the photoelectric emission of electrons from a surface, or electronic transitions in semiconductor materials. Therefore, the output of photon sensors depends on the photon's absorption rate and not directly on photon energy. They normally require to be cooled to cryogenic temperatures in order to get rid of excessive dark current, but have high performance, with larger detectivities and smaller response times. They respond only to photons whose energy $h\nu$ is equal to or larger than the energy gap or than the ionization energy. The rate of carrier generation due to a given incident power P is given by:

$$G(s^{-1}) = \eta P/h\nu \tag{1}$$

for $h\nu \geq Eg$, and $G = 0$ for $h\nu \leq Eg$. If τ does represent the lifetime of the carriers in a photoconductor we have $\Delta n = G\tau$, while in photovoltaic sensors the current is given by $I = qG$.

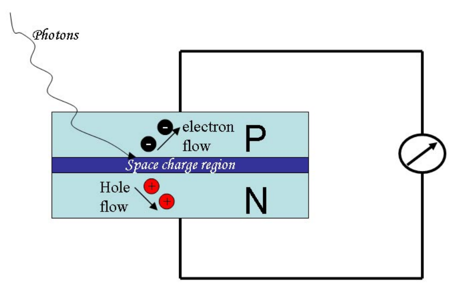

(a) Photovoltaic device.

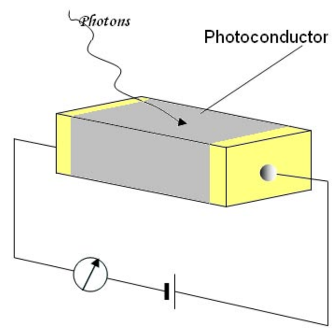

(b) Photoconductive device.

Fig. 1. Photon sensors

Photon sensors can be further subdivided into *photoconductive* and *photovoltaic* devices. The function of photoconductive sensors are based on the photogeneration of charge carriers (electrons, holes or electron-hole pairs). These charge carriers increase the conductivity of the device material. Detector materials possible to be utilized for photoconductive sensors are:

- Indium Antimonide($InSb$)
- Quantum Well Infrared Photodetector (QWIP)
- Mercury Cadmium Telluride ($Hg_xCdTe_{(1-x)}$)
- Lead Sulfide (PbS)
- Lead Selenide ($PbSe$)

- Lead Tin Telluride ($Pb_xSnTe_{(1-x)}$)

Photovoltaic devices (figure 1(a)) require an internal potential barrier which derives from the presence of a built-in electric field in order to be able to separate the photo-generated electron-hole pair. Such potential barriers can be created by the use of p-n junctions or Schottky barriers. While the current-voltage characteristics of photoconductive devices are symmetric with respect to the polarity (if we neglect small deviation due to the presence of delocalized space charge regions at the contacts or inside the non perfect material) of the applied voltage, photovoltaic devices exhibit rectifying behavior. Photon sensors may also be classified on the basis of whether the photo-transitions take place across the fundamental band gap of the infrared sensitive material, or from impurity states to either of the valence or the conduction band. In the first case they are denoted *intrinsic*, in the latter case *extrinsic*. The quantum well type of detector discussed below is however not easily classified according to this criterion. (See fig. 2).

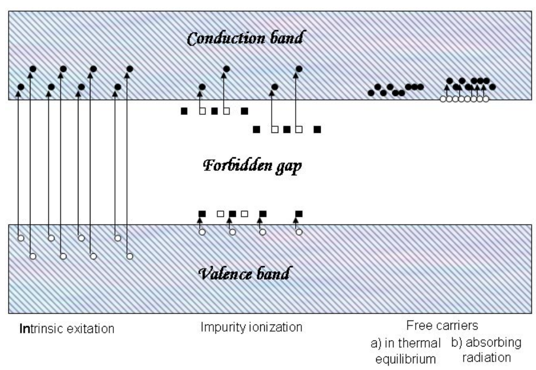

Fig. 2. Photoconductivity processes showing the electron transitions in four different cases.

In most cases photon sensors need to be cooled to cryogenic temperatures, i.e. down to $77K$ (liquid nitrogen) or $4K$ (liquid helium). In some favorable cases thermoelectric cooling down to $200K$ is sufficient (e. g. $3-5\mu m$ wavelength mercury cadmium telluride). The main workhorse in the field of photon sensors is mercury cadmium telluride ($HgCdTe$), and to a less extent indium antimonide ($InSb$). Vigorous work has been done on cadmium telluride both in the US and Europe since its discovery in 1959 and work is still being done. Cadmium telluride is used both for the $3-5\mu m$ (MWIR) and $8-12\mu m$ (LWIR) atmospheric transmission windows, whereas indium antimonide is only used for the $3-5\mu m$ range. Platinum silicide ($PtSi$) Schottky barrier sensors also work in the MWIR domain. Large (512x512 pixels) $PtSi$ focal plane arrays have been fabricated, they are compatible with silicon CCD/CMOS technology, and show high performance, due to the extremely good pixel to pixel uniformity, in spite of the very low quantum efficiency. As regards FPAs for the $3-5\mu m$ window, both cadmium telluride, $InSb$ and $PtSi$ materials pose no major technological problems and are considered to be a finished product. In contrast, to date, no photon sensors FPAs operating in the $8-12\mu m$ window exhibit sufficient performance to be operated at $77-80K$. In the course of only the last five years, sensors based on low-dimensional structures have evolved as viable candidates for FPAs (focal plane arrays), especially in the LWIR region. These so called band-gap engineered sensors operate on account of electronic transitions between electronic states arising as a result of size quantization, i.e. electron energy quantization due to the small layer dimensions in the growth direction. There are three main candidates of interest for IR sensor arrays:

i) the $AlGaAs/GaAs$ quantum wells
ii) the strained $SiGe/Si$ superlattices (SL)
iii) the strained InAs/GaInSb SLs and others

Among them the most mature is the $AlGaAs/GaAs$ quantum well (QW) structure, which is a spin-off from $GaAs$ technology. This sensor type is generally named Quantum Well Infrared Photoconductor or QWIP. Here special grating structures are necessary in order to achieve a high quantum efficiency of the detector. QWIP FPAs need operating temperatures around $70-75K$ in order to work properly, temperatures which are easily achievable by miniature Stirling coolers. The main advantages of SiGe/Si QWs are the compatibility with silicon technology and that grating structures are not necessary. The cooling requirements seem, however, to be more extensive than for $AlGaAs/GaAs$ quantum wells. InAs/GaInSb so called type II SLs in theory offer the possibility of high sensitivity and operating temperatures of an intrinsic detector. In addition, the materials processing and uniformity are expected to be superior to that of III-VI materials such as cadmium telluride. However, presently the maturity of the sensor technology is far from being comparable to cadmium telluride sensors.

3.3 Thermal sensors

In contrast to photon sensors, the operation of thermal sensors is straightforward . The absorption of infrared radiation in these sensors raises the temperature of the device, which in turn changes some temperature-dependent parameter such as electrical conductivity, gas pressure or thermal polarizability. All these kinds of thermal sensors show a remarkably flat response of the detectivity versus the wavelength (see fig. 3). Thermal sensors may be thermopile (Seebeck effect), bolometer, Golay cell sensors, thermopile or pyroelectric sensors ($LiTaO_3$). This last sensor deserves a remark; in fact the current generated in a given load resistor is proportional to the average temperature

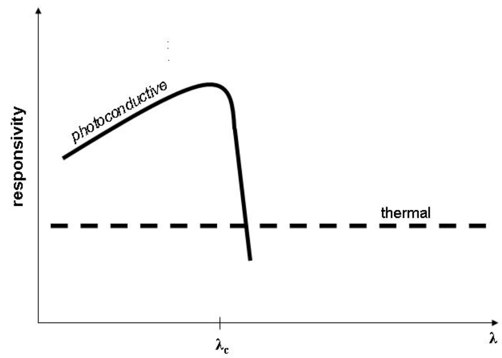

Fig. 3. Theoretical response of thermal and photosensors

rate and for this reason it is sometimes called a derivative temperature detector. If p represents the pyroelectric coefficient and A is the detector area, the current is given by:

$$I = p \cdot A \cdot \frac{d(< T >)}{dt}. \tag{2}$$

The most relevant advantage of thermal sensors is that they can operate at room temperature. However, the detectivity is lower and the response time longer than for photon sensors. This makes thermal sensors suitable for focal plane array operation, where the latter two properties are less critical.

A thermal detector is conveniently divided into three functional parts:

- Absorber for infrared radiation
- Membrane or other structure for achieving thermal insulation
- Temperature detector

The *absorber* can be a finely subdivided metal such as platinum black, or be based on an interferometric structure. A simple model useful to understand the operating principle of a thermal detector is shown in fig. 4. From this figure it is possible to derive the heat equation of this device which can be expressed as follows:

$$C \cdot \frac{d(\Delta T)}{dt} + G \cdot \Delta T = Re[W \cdot e^{j\omega t}] \tag{3}$$

where:

- C is the heat capacity of the detector
- G is the thermal conductance between the sensor and the heat sink at temperature T_0
- W is the adsorbed peak power
- ω is the angular modulation frequency

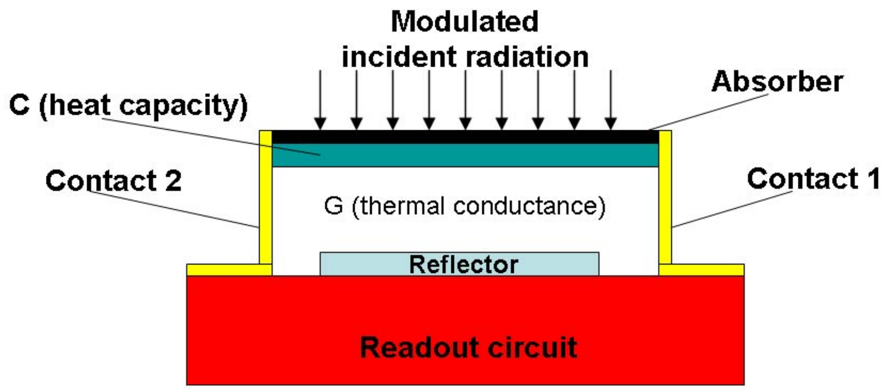

Fig. 4. Thermal detector.

Leaving out the mathematical details the solution of the heat equation rewritten as:

$$\frac{d(\Delta T)}{dt} + \frac{\Delta T}{\tau} = Re[\frac{W}{C} \cdot e^{j\omega t}] \tag{4}$$

which considers the modulated response is given by:

$$\Delta T = (\frac{W}{C} \cdot e^{j\omega t}) \cdot (1 + j\omega t) \tag{5}$$

where $\tau = \frac{C}{G}$ is the thermal time constant of the device. The real time dependence of the temperature change versus the frequency is then given by:

$$\Delta T = \frac{W}{G} \cdot \frac{1}{\sqrt{1 + \omega^2 \tau^2}}. \tag{6}$$

If $\omega\tau$ is less than 1 the temperature rise does not depend on the heat capacity C which is usually minimized for achieving fast responses. In order to obtain high sensitivity it is of utmost importance that the detector element is thermally insulated from the detector substrate. Therefore, when fabricating thermal detector arrays it is common to make thin membranes using micro-mechanical processing techniques. The material may be silicon nitride or silicon dioxide, which both are compatible with silicon processing techniques.

The *temperature detector* is usually integrated into a suitable membrane, and utilized to detect the usually minute temperature change resulting from exposure to infrared radiation from a room-temperature scene and subsequent absorption. Thermal sensors are conveniently classified according to their means of detecting this temperature change:

- A resistive bolometer contains a resistive material, whose resistivity changes with temperature. To achieve high sensitivity the temperature coefficient of the resistivity should be as large as possible and the noise resulting from contacts and the material itself should be low. Resistive materials could be metals such as platinum, or semiconductors (thermistors). Metals usually have low noise but have low temperature coefficients (about $0.2\%/K$), semiconductors have high temperature coefficients ($1 - 4\%/K$) but are prone to be more noisy. Semiconductors used for infrared sensors are e.g. amorphous, polycrystalline silicon, or vanadium oxide.
- A thermoelectric device (thermocouple or thermopile) is based on the presence of one or several junctions between two materials. The junctions properly arranged and connected develop a *thermo-emf* that changes with temperature, the so-called Seebeck effect. In order for the sensitivity to be high the Seebeck coefficient should be as high as possible. Certain alloys containing antimony and bismuth have very high Seebeck coefficients of $150\mu V/K$. The CMOS compatible combination aluminum/polycrystalline silicon gives about $65\mu V/K$.
- A pyroelectric sensor is based on the fact that certain dielectric materials of low crystal symmetry exhibit spontaneous dielectric polarization. When the electric dipole moment depends on temperature the material becomes pyroelectric. Usually a capacitor is fabricated from the material and the variation of charge on it is sensed. Common pyroelectric materials used for infrared sensors are TGS (tri-glycine sulphate), $LiTaO_3$ (lithium tantalate), PZT (lead zinc titanate) and certain polymers.A *dielectric bolometer* makes use of pyroelectric materials operated in a way to detect the change of the dielectric constant with temperature. A suitable material for this application is SBT (Strontium Barium Titanate).
- The Golay detector is based on the volume or pressure change of an encapsulated gas with temperature. The volume change is measured e.g. by the deflection of light rays resulting from the motion of properly positioned mirrors fastened to the walls of the gas container.

3.4 Infrared Imaging

There are two basic types of infrared imaging systems: mechanical *scanning systems* and systems based on detector arrays without a scanner. It should be mentioned that *detector arrays* as well are used for scanning systems, but the number of detector elements (picture elements - pixels) generally is smaller in this case.

A mechanical *scanner* utilizes one or more moving mirrors to sample the object plane sequentially in a row-wise manner and project these onto the detector. The advantage is that only one single detector is needed. The drawbacks are that high precision and thus expensive opto-mechanical parts are needed, and the detector response time has to be short. As mentioned above, detector arrays are also used for this application. For example, a long linear detector array can be used to simultaneously sample one column of the object plane. By using a single moving mirror the whole focal plane can be sampled. In contrast, when a single detector is used, two mirrors moving in two orthogonal directions must be used, one of them moving at high speed, the other one at lower speed.

Detector arrays operated as *focal plane arrays* (FPA) (or *staring arrays*) are located in the focal plane of a camera system, and are thus replacing the film of a conventional camera for visible light. The advantage is that no moving mechanical parts are needed and that the detector sensitivity can be low and the detector slow. The drawback is that the detector array is more complicated to fabricate. However, rational methods for semiconductor fabrication yield economic advantages, provided that production volumes are large. The general trend is that infrared camera systems will be based on FPAs, except for special applications.

The spatial resolution of the image is determined by the number of pixels of the detector array. Common formats for commercial infrared sensors are 320x240 pixels (320 columns, 240 rows), and 640x480. The latter format (or something close to it), which is nearly the resolution obtained by standard TV, will probably become commercially available in the next few years. Today, for example, indium antimonide and platinum silicide sensors are commercially available in the 320x240 pixels format. Typical pitches between pixels are in the range $20 - 50\mu m$.

Detector arrays are more complicated to fabricate, since besides the detector elements with the function of responding to radiation, electronic circuitry is needed to multiplex all the detector signals to one or a few output leads in a serial manner. The output from the array is either in analogue or digital form. In the former case analogue to digital conversion is usually done external to the detector array. The electronic chip used to multiplex or read out the signals from the detector elements are usually called simply *readout integrated circuit* (ROIC) or (analogue) multiplexer.

The ROIC is usually made using silicon CCD (charge coupled device) or CMOS technology. However, the detector elements must often be fabricated from more exotic materials as discussed above. The exceptions are e. g. platinum silicide or micro-bolometers which can be based on silicon technology. In the former case a hybrid approach is most common, in which case all the detector pixels are fabricated from a separate detector chip. This detector chip is then *flip-chip bonded* to the ROIC chip. Flip-chip bonding involves the processing of metal bumps onto contact holes, one per pixel, of both the detector chip and the ROIC . Using special equipment, the two chips are first aligned to each other. Then the chips are put in contact, while applying heat and/or mechanical force. During this process the two chips become electrically connected to each other via the metal bumps. Usually indium is used for the bumps due to its excellent low temperature properties.

Uniformity of the detector elements across the array is a key issue for obtaining high performance. In fact, individual pixel response characteristics differ considerably across an array in most cases. Therefore so called pixel correction has to be done prior to the presentation of the final image. This amounts to calibrating each individual pixel, by exposing the array to calibrated surfaces of known temperature.

IR sensor can be divided in two broad categories: incoherent and coherent. Incoherent infrared sensors can be seen as sensors sensitive to the photon energy. Examples are: photomultiplier , photoconductors, bolometers, etc. For all of them in the detection process, information of phase and frequency is lost. Coherent IR sensors are all those that can maintain frequency and phase information; examples are linear amplifiers heterodine sensors (mixers).

4 Figure of merit of incoherent IR sensors (I.I.R.S.)

The most important figures of merit for I.I.R.S. are:

4.1 Noise equivalent Power (NEP)

It is defined as the r.m.s. value of a sinusoidally modulated radiant power falling on the sensor able to determine signal to noise ratio equal to unity.
The NEP (or P_N) depends on the (S/N) noise bandwidth of the preprocessing circuit.
The smaller this bandwidth, the lower the NEP. The NEP is given with reference to 1 Hz bandwidth ($W/\sqrt{Hz}$).
The NEP should be written as follows:
NEP (500K, 900, 1) where, as an example, 500K represents the Black Body temperature, 900 is the chopping frequency, and 1Hz is the bandwidth.
P_N can be experimentally estimated by the following relationship:

$$P_N(or NEP) = I \cdot A_S \cdot \frac{V_n/V_s}{\sqrt{\Delta f}} \tag{7}$$

where I is the irradiance falling on the sensor area A_S, (V_n/V_s) is the noise to signal ratio evaluated in the bandwidth (Δf).

4.2 Responsivity

It can be represented by the electrical output of a sensor divided by the power (P) of the radiation striking it. Since electrical output can be either voltage or current, one distinguishes between voltage and current responsivity.

$$R = \frac{V_s}{P} = \frac{V_s}{I \cdot A_s}. \tag{8}$$

The responsivity unit is $[V/W]$.

It is worth underlining that the responsivity is linked to the NEP and to the D^* as follows:

$$R = \frac{V_n}{P_N \cdot \sqrt{\Delta f}} = \frac{D^* \cdot V_n}{\sqrt{A_s \cdot \Delta f}}. \tag{9}$$

It is relevant also to mention that the responsivity is frequency dependent and in most cases its behaviour can be expressed as follows:

$$R(f) = \frac{R_0}{\sqrt{1 + \omega^2 \tau^2}}. \tag{10}$$

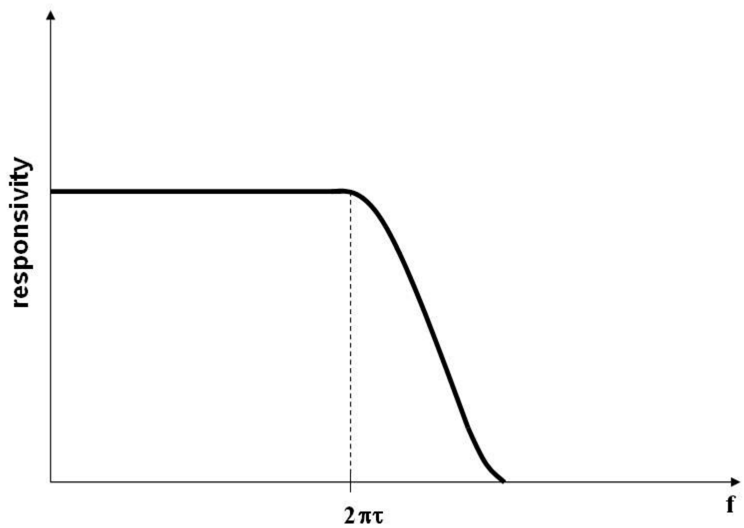

Fig. 5. Frequency dependence of the responsivity.

Responsivity can be measured for monochromatic radiation, in which case the responsivity is called spectral responsivity. Alternatively, a blackbody source kept at a fixed temperature can be used. In this case one talks about black body responsivity. Spectral responsivity plotted versus wavelength is often used for presentation of a detector's spectral response properties.

4.3 Detectivity D^*

Whereas responsivity takes into account the detector's signal properties only, the detectivity or D^* value is a measure of its signal to noise properties. The D^* value is normalized with respect to detector area (provided that the signal to noise ratio increases with the square root of the detector area, which is often the case, at least for photon sensors). It is defined as:

$$D^* = \frac{R}{V_N} \cdot \sqrt{A_S \cdot \Delta f} = \frac{R}{I_N}\sqrt{A_S \cdot \Delta f} \tag{11}$$

where V_N and I_N is the noise voltage and current, respectively, R is the responsivity, A_S the detector area and Δf the noise bandwidth.

4.4 Temperature resolution (NETD) and other important parameters

NETD is an abbreviation for Noise Equivalent Temperature Difference and is a measure of the smallest object temperature difference that can be detected by an IR camera.
When dealing with I.R. sensors also the following parameters are important:

- *Operating temperature:* temperature of the I.R. sensor;
- *Cut-Off wavelength:* wavelelength above which the response goes to zero;
- D_{λ_p}*:* which is similar to the normal D^* apart from the fact that here the input power is related to a small $\Delta\lambda$ generated, for instance, by a monochromator;
- *Response time:* time which goes from 0.1 to 0.9 of the overall response;
- *Noise mechanism:* which describes the kind of noise (shot, thermal, flicker, burst);
- *Resistance/squares:* representing a measure of a thin film of sensitive material;
- *Mode of operation:* describes how the device is applied and how the output voltage (current) is taken.

Figure 6 gives a broad representation of the most important infrared sensors in terms of detectivity (D^*) versus wavelengths. Only a few sensors, namely pyroelectric, Golay cell, thermopile, thermistor (letters S-T-U-V), have a flat response from the visible to above 20 μm. Other sensors (letters A-B-C-D-E-F-G-H-R-I-J-L-R-O) have a band pass behaviour in the one to five microns region, others (K-N-M-Q) show broad response covering many microns of range. The envelope of all the curves are located below the ideal limit of both photoconductive and photovoltaic sensors.

When IR sensors are taken into consideration it is worth keeping in mind the following radiation terms:

- Radiant power: P (Watts)
- Spectral radiant power: P_λ(W/μm)
- Radiant intensity: I (W/steradiants)
- Spectral radiant intensity: I_λ (Watts/steradiant. μm)
- Radiant emittance: R_e (W/m^2)
- Spectral radiant emittance: $R_{e\lambda}$ $(W/m^2 \cdot \mu m)$
- Radiance: R_Ω $(W/m^2 \cdot steradiant)$
- Spectral radiance: $R_{\Omega\lambda}$ $(W/m^2 \cdot steradiant \cdot \mu m)$

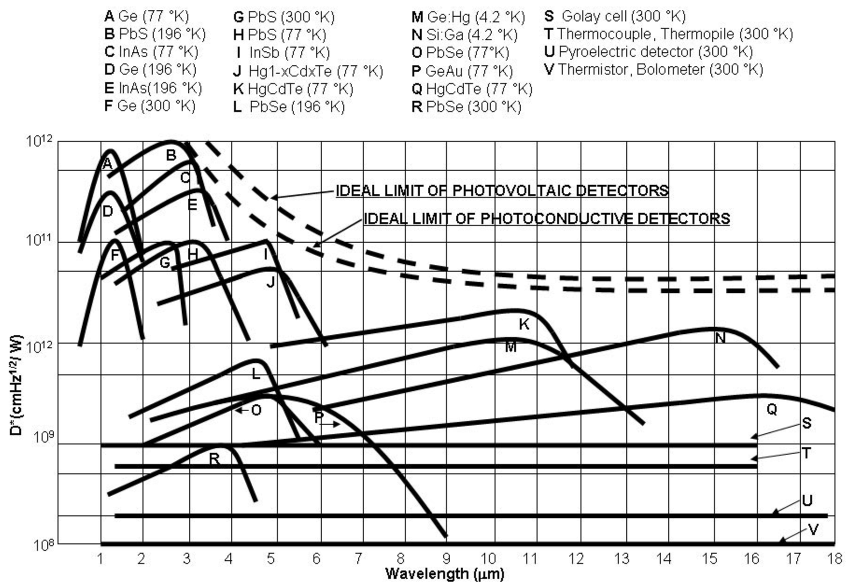

Fig. 6. Detectivity versus wavelength in the infrared region of different sensors.

- Irradiance: I_R (W/m^2)
- Reflectivity (R); Absorptivity(α); Transmittivity(T); Emissivity(E): which are all expressed by numbers, each less than one, in practical cases.

After this brief introduction to IR sensors we will talk about the acousto-optic technique which seems to be suitable for the detection of aggressive volatile compounds in the $8 - 14\mu m$ region. Below we list a number of aggressive compounds to which a great deal of attention is paid:

- **Nerve Agents:** Sarin, Ciclosarin, Tabun, Soman, VX;
- **Blister Agents:** Nitrogen Mustards (HN-1, HN-2, HN-3), absorption @ $14\mu m$;
- **Pulmonary Agents:** Cloropicrina, Perfluoro-Isobutilene (PFIB), Fosgene;
- **Blood Agents:** CNCl.

5 Acousto-optic devices

The early studies on acousto-optic phenomena, i.e. the optical interactions with acoustic waves, go back to around the 1920s, as pointed out by C.F. Quate and M. Born in their articles [2, 37]. The acousto-optic interactions occur in an optical media (usually solid, sometimes liquid, rarely a gas) when an optic wave and an acoustic wave are present in the same place and time. The strain of the medium due to the pressure fluctuation of the acoustic wave causes diffraction, refraction, interference and reflection of the optical wave. After the advent of the laser acousto-optics research was especially dedicated to the development of devices able to modulate and deflect the laser beam [7, 12, 20]. Here we develop a bit of theory, taken from the literature, related to the acousto-optic mechanism and give some explanations of some related devices, essential for the generation of power in relatively small $\Delta\lambda$, to be used in volatile compound absorption based detection techniques.

5.1 Acousto-optic interaction theory

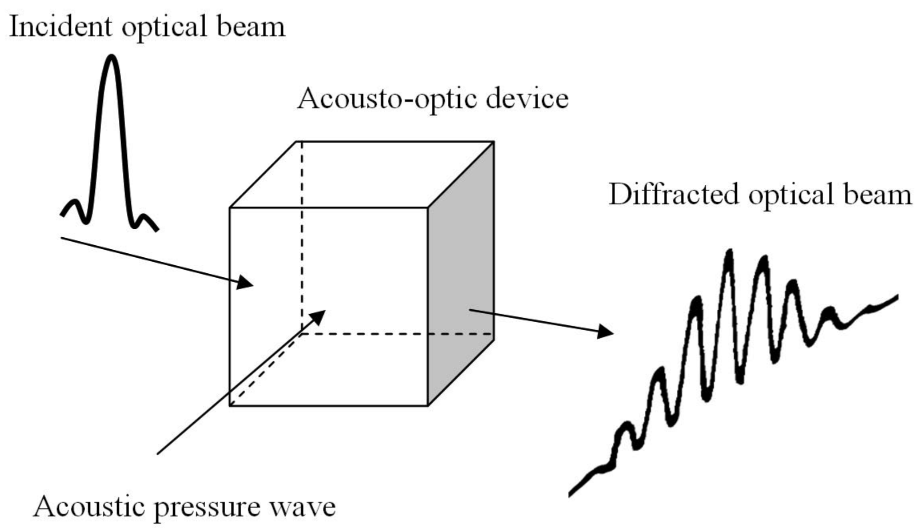

Fig. 7. Scenario.

5.1.1 The Elasto-optical effect

Let $\mathbf{E}(\mathbf{r}, t)$ and $\mathbf{H}(\mathbf{r}, t)$ be respectively the electric field and the magnetic field of the light beam. Thus Maxwell's equation within the medium can be written as

$$\nabla \times \mathbf{E} = -u_0 \frac{\partial}{\partial t} \mathbf{H} \tag{12}$$

$$\nabla \times \mathbf{H} = \frac{\partial}{\partial t} (\varepsilon \mathbf{E}) \tag{13}$$

$$\mathbf{D} = \varepsilon \mathbf{E} \tag{14}$$

$$\nabla \cdot \mathbf{D} = \rho = 0 \tag{15}$$

by Gauss' law. The optical properties of a medium are completely characterized by the electric impermeability tensor $\boldsymbol{\beta} = \varepsilon_0 \boldsymbol{\varepsilon}^{-1}$ (not to be confused with the impedance of the medium), where $\boldsymbol{\varepsilon}^{-1}$ is the inverse of the tensor $\boldsymbol{\varepsilon}$. So equation (14) can be inverted and rewritten as

$$\varepsilon_0 \mathbf{E} = \boldsymbol{\beta} \mathbf{D}. \tag{16}$$

In the directions for which $\mathbf{E}$ and $\mathbf{D}$ are parallel, both tensor $\boldsymbol{\varepsilon}$ and $\boldsymbol{\beta}$ share the same principal axes and are represented by a diagonal matrix. Thus the principal values of $\boldsymbol{\beta}$ are

$$\frac{\varepsilon_0}{\varepsilon_1} = \frac{1}{n_1^2}; \frac{\varepsilon_0}{\varepsilon_2} = \frac{1}{n_2^2}; \frac{\varepsilon_0}{\varepsilon_3} = \frac{1}{n_3^2} \tag{17}$$

where $\varepsilon_1 = \varepsilon_{11}$, $\varepsilon_2 = \varepsilon_{22}$ and $\varepsilon_3 = \varepsilon_{33}$.

The quadratic representation of the electric impermeability tensor $\boldsymbol{\beta}$

$$\sum_{ij} \beta_{ij} x_i x_j = 1 \qquad i,j=1,2,3 \tag{18}$$

is called the index ellipsoid or optical indicatrix. Using principal axes as the coordinate system the quadratic form is described by

$$\frac{x^2}{n_x^2} + \frac{y^2}{n_y^2} + \frac{z^2}{n_z^2} = 1. \tag{19}$$

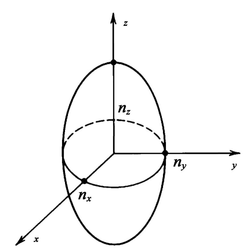

Fig. 8. The index ellipsoid.

For example, if the medium is isotropic then the indicatrix will describe a spherical surface or, if it is a uniaxial crystal, the surface will be an ellipsoid of revolution [26].

When the medium is perturbed by a sound wave $\mathbf{S}(\mathbf{r}, t)$, the compression and refraction waves change the local density and the resulting strain of the component atoms and molecules of the scattering medium change the optical polarization [12].

As a consequence the permittivity tensor $\boldsymbol{\varepsilon}$ changes its coefficients, and hence β too according to the equation

$$\beta_{ij} = \beta_{0_{ij}} + \Delta\beta_{ij}, \tag{20}$$

where

$$\Delta\beta_{ij} = p_{ijkl} S_{kl} \qquad i,j,k,l=1,2,3. \tag{21}$$

$\Delta\beta_{ij}$ is the variation due to the perturbation, $\beta_{0_{ij}}$ is the indicatrix coefficient before the perturbation and p_{ijkl} are the elastooptic or photoelastic constant coefficients of the strain-optic tensor of fourth rank. They reflect a particular symmetry due to symmetry both of $\Delta\beta_{ij}$ and of S_{kl}, in particular $p_{ijkl} = p_{jikl} = p_{ijlk}=p_{jilk}$ [22, 41]. In this way it is possible to contract the pair of indices (i,j) to a single index m=1,2,. . . ,6 using the Nye's notation reported at table (1) [42]. Also the pair of indices (k,l) can be contracted to the index n=1,2,. . . ,6 in the same way. For example the pair (k, l) = (1,2) is labeled n=6.

j	i:1	2	3
1	1	6	5
2	6	2	4
3	5	4	3

Table 1. Lookup table for the index m or n that represents the pair of indices (i,j) or (k,l).

Moreover the symmetry of the crystal adds other constraints on the coefficients. For example the matrix *pmn* of a cubic crystal [36, 42] has the structure

$$pmn=\begin{bmatrix} p_{11} & p_{12} & p_{12} & 0 & 0 & 0 \\ p_{12} & p_{11} & p_{12} & 0 & 0 & 0 \\ p_{12} & p_{12} & p_{11} & 0 & 0 & 0 \\ 0 & 0 & 0 & p_{44} & 0 & 0 \\ 0 & 0 & 0 & 0 & p_{44} & 0 \\ 0 & 0 & 0 & 0 & 0 & p_{44} \end{bmatrix}.$$

Furthermore if the medium material is isotropic

$$p_{44} = \frac{1}{2}\left(p_{11} + p_{12}\right). \tag{22}$$

Other photoelastic matrices for different types of crystal have been published by Mason [27], Nye [34] and Krishnan [24].

Table 2 reports some elastoplastic coefficients. More detailed tables can be found in [8, 46].

For example, let us now consider a longitudinal acoustic wave characterized by a displacement $u_x = A_0 \sin(\omega_{ac} t - k_{ac} x)$, $u_y = 0$ and $u_z = 0$, traveling into an isotropic cubic crystal ($n_{0x} = n_{0y} = n_{0z}$) along the x direction. Thus the strain tensor S_{ij} , defined as

Material	l(mm)	n	P_{11}	P_{12}	P_{44}	P_{31}	P_{13}	P_{33}	P_{41}	P_{14}	P_{66}
Fused quartz	0.63	1.46	0.121	0.270	-0.075						
GaP	0.63	3.31	-0.151	-0.082	-0.074						
GaAs	1.15	3.37	-0.165	-0.140	-0.072						
TiO_2	0.63	2.58	0.011	0.172		0.0965	0.168	0.058			
$LiNbO_3$	0.63	2.20	0.036	0.072		0. 178	0.092	0.088	0.155		
$LiTaO_3$	0.63	2.18	0.0804	0.0804	0.022	0.086	0.094	0.150	0.024	0.031	
KDP	0.63	1.51	0.251	0.249		0.225	0.223	0.246			0.058
H_2O		1.33	0.31								

Table 2. Elastoplastic coefficients and refractive index

$$S_{ij} = \frac{1}{2}\left(\frac{\partial u_i}{\partial x_j} + \frac{\partial u_j}{\partial x_i}\right) \tag{23}$$

where i,j = 1,2,3 denotes the coordinate (x,y,z), which has all components vanishing except

$$\mathrm{S}_{11} = S_1 = \mathrm{S}_0\cos(\omega_{ac}t - k_{ac}x) = -k_{ac}A_0\cos(\omega_{ac}t - k_{ac}x). \tag{24}$$

By substituting (24) and (20) into (21) we find

$$\beta_{11} = \frac{1}{(n_x)^2} + p_{11}S_1 \tag{25}$$

$$\beta_{22} = \beta_{33} = \frac{1}{(n_x)^2} + p_{12}S_1 \tag{26}$$

$$\beta_{ij} = 0,\ i \neq j. \tag{27}$$

Equations (25), (26), (27) show that the initial isotropic crystal has become a uniaxial crystal (two refractive index are equal) and the quadratic form of the optical indicatrix represents an ellipsoid of revolution whose axes $n_o = n_2 = n_3$ and $n_e = n_1$ are given by

$$\frac{1}{(n_o)^2} = \frac{1}{\left(n_{0_x}\right)^2} + p_{12}S_1 \tag{28}$$

$$\frac{1}{(n_e)^2} = \frac{1}{\left(n_{0_x}\right)^2} + p_{11}S_1 \tag{29}$$

where n_o and n_e represent the ordinary and extraordinary refractive index. Using the approximation

$$\frac{1}{\sqrt{1+a}} \approx 1 - \frac{1}{2}a \quad with \quad a \ll 1 \tag{30}$$

it is possible to write (28) or (29), with $i = e, o$ as

$$n_i = \frac{n_{0_x}}{\sqrt{1+(n_{0_x})^2 p_{mn} S_m}} = n_{0_x}\left[1 - \frac{1}{2}(n_{0_x})^2 p_{mn} S_m\right]$$

$$= n_{0_x} - \frac{1}{2}(n_{0x})^3 p_{mn} S_m \tag{31}$$

and hence

$$\Delta n_i = n_i - n_{0_x} = -\frac{1}{2}(n_{0_x})^3 p_{mn} S_m. \tag{32}$$

The variation of the reflective index Δn is negative compared with the positive strain perturbation S. Other than the longitudinal wave, also, the transverse share wave is very common in acousto-optic devices. Here the displacement wave, $u_x = 0$, $u_y = 0$ and $u_z = A_0 \sin(\omega_{ac} t - k_{ac} x)$, travels in an isotropic cubic crystal along the x direction but vibrates orthogonally in the z direction. Thus the strain tensor has all components zero except

$$S_{13} = S_{31} = S_5 = S_0 \cos(\omega_{ac} t - k_{ac} x) = -\frac{1}{2} k_{ac} A_0 \cos(\omega_{ac} t - k_{ac} x) \tag{33}$$

and the crystal will become biaxial (the three principal indices are different from each other). Reassembling (32) and using (33), the principal refractive index will be given by

$$n_x = n_{0_x} - \frac{1}{4}(n_{0_x})^3 k_{ac} A_0 \cos(\omega_{ac} t - k_{ac} x) \tag{34}$$

$$n_y = n_{0_x} \tag{35}$$

$$n_z = n_{0_x} + \frac{1}{4}(n_{0_x})^3 k_{ac} A_0 \cos(\omega_{ac} t - k_{ac} x). \tag{36}$$

If we want to consider the variation of the permitivity $\boldsymbol{\epsilon}$ related to the photoelastic effect we can write [23, 44]

$$\boldsymbol{\epsilon}(\mathbf{r}, t) = \varepsilon_0 (1 + C\mathbf{S}(\mathbf{r}, t)) = \varepsilon_0 + \boldsymbol{\epsilon}'(\mathbf{r}, t), \tag{37}$$

where $\boldsymbol{\epsilon}(\mathbf{r}, t) = \varepsilon_0 C\mathbf{S}(\mathbf{r}, t)$ is the time-varying permitivity and C is a constant dependent on the medium material.

Furthermore, if we assume that the acoustic wave is a planar traveling wave with sinusoidal vibration, then the relationship between the variation of the refractive index D*n(x,t)* and the acoustic strain wave can be written as [21]

$$\Delta n(x, t) = \frac{n}{2} C S(x, t) \tag{38}$$

and

$$C = -n^2 p. \tag{39}$$

Note that the above (39) defines the constant C using the refractive index n as a scalar, and hence (39) can usually be applied to a liquid [40].

5.1.2 Raman-Nath diffraction

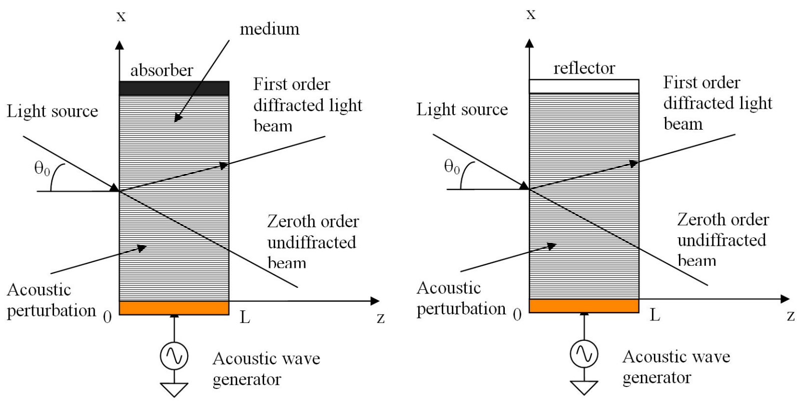

(a) Propagation acoustic wave. (b) Standing acoustic wave.

Fig. 9. Schematic of Acousto-optic devices

Let us consider now a progressive sinusoidal perturbation wave $\mathbf{S}(\mathbf{r},t)$ propagating into an optical medium large L and width W, characterized by a permeability μ_0 and a permitivity $\boldsymbol{\epsilon}$, and the electric field $\mathbf{E}(\mathbf{r},t)$ incident at an angle θ_0 upon the acoustic beam as shown in figure 9(a) and 9(b). In order to model the acousto-optic interaction we have to consider the Maxwell equation stated above considering $\boldsymbol{\epsilon}$ as a function of x, y, z coordinates and time t. Eliminating $\mathbf{H}$, we obtain [31]

$$u_0 \varepsilon_0 \frac{\partial^2 \mathbf{D}}{\partial t^2} = \nabla^2 \mathbf{E} + \frac{\nabla \boldsymbol{\epsilon}}{\boldsymbol{\epsilon}} \nabla \times \mathbf{E} + \left(\frac{\nabla \boldsymbol{\epsilon}}{\boldsymbol{\epsilon}} \nabla \right) \mathbf{E} + (\mathbf{E} \nabla) \frac{\nabla \boldsymbol{\epsilon}}{\boldsymbol{\epsilon}}. \tag{40}$$

Since $\omega_{ac} << \omega_{op}$

$$|\nabla \boldsymbol{\varepsilon}| \, \lambda << 1. \tag{41}$$

Thus (40) can be written as

$$\nabla^2 \mathbf{E} - \mu_0 \varepsilon_0 \frac{\partial^2}{\partial t^2} (\boldsymbol{\epsilon} \mathbf{E}) = 0 \tag{42}$$

Hence, assuming that the frequency of time variation of $\boldsymbol{\epsilon}$ is very small compared to that of $\mathbf{E}$, (42) is reduced to

$$\nabla^2 \mathbf{E} = \mu_0 \boldsymbol{\epsilon} \frac{\partial^2}{\partial t^2} (\mathbf{E}) \quad or \quad \nabla^2 \mathbf{E} = \frac{\mathbf{n}(\mathbf{r}, t)^2}{c^2} \frac{\partial^2}{\partial t^2} (\mathbf{E}) \tag{43}$$

where c is the light velocity in free space and $\mathbf{n}(\mathbf{r}, \mathrm{t}) = \frac{\mathbf{c}}{c_{medium}(\mathbf{r}, t)}$ is the refracting index of the medium [46].

Let $\mathbf{S}(\mathbf{r},\mathrm{t})$ be the sinusoidal perturbation propagating along the x axis, so $\mathbf{S}(\mathbf{r},\mathrm{t})$ can be written as

$$S(x, t) = \frac{1}{2} S_0 \exp\left[j(\omega_{ac} t - k_{ac} x)\right] + c.c. \tag{44}$$

and let $\mathbf{E}(\mathbf{r}, t)$ be defined as

$$\mathbf{E}(\mathbf{r}, t) = \frac{1}{2} E_{op}(r) \exp\left[j(\omega_{op} t - \mathbf{k_{op}} \cdot \mathbf{r})\right] + c.c. \tag{45}$$

where S_0 is the amplitude of the perturbation, E_{op} is the amplitude in free space and *c.c.* is the complex conjugate. Furthermore let *n(x,t)* be the refractive index of the medium perturbed in time and space by the pressure acoustical wave, given by

$$n(x, t) = n_0(x) + \Delta n(x, t) \tag{46}$$

where $\Delta n(x, t)$ can be written according to (32) as

$$\Delta n(x, t) = -\frac{1}{2} (n_0)^3 \, p S_0 \sin(\omega_{ac} t - k_{ac} x). \tag{47}$$

As the scattering process is essentially lossless, or reactive, the wave energy-momentum conservation principles are applicable. In the case of a plane monochromatic optical and acoustic wave propagated in a medium that is optically inhomogeneous, nonmagnetic and isotropic, the energy-momentum relations are given by

$$\hbar k_s = \hbar k_{op} + \hbar k_{ac}$$

$$\hbar \omega_s = \hbar \omega_{op} + \hbar \omega_{ac}$$

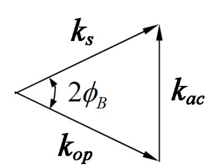

Fig. 10. Momentum scattering of a plane and monochromatic optical and acoustic waves in isotropic medium.

where the subscript s means scattered, $\hbar$ is Planck's constant h divided by 2π, k_s, k_{ac} and k_{op} are respectively the scattered, acoustic and optic wave vector, and k_{ac} and k_{op} are defined as $k_{ac} = \frac{\omega_{ac}}{v_{ac}}$ and $k_{op} = \frac{\omega_{op}}{v_{op}} = \frac{\omega_{op} n_0}{c}$.

Figure 10 shows the vector representation of the moment conservation. Along the interaction area, the perturbed optical field $\mathbf{E}$ can be written as [5, 18, 46]

$$E(x,z,t) = \frac{1}{2}\sum_{m=-\infty}^{+\infty} E_m(z)\exp\left[j(\omega_m t - \mathbf{k}_m \cdot \mathbf{r})\right] + c.c. \tag{48}$$

where

$$\omega_m = \omega_{oc} + m\omega_{ac} \tag{49}$$

$$\mathbf{k}_m = k_{op} + mk_{ac} \tag{50}$$

$$\mathbf{k}_m \cdot \mathbf{r} = k_{op}[z\cos(\vartheta_0) - x\sin(\vartheta_0)] + mk_{ac}x. \tag{51}$$

$E_m(z)$ represents the amplitude of the m^{th} diffracted light with circular frequency $\omega_m = \omega_{op} + m\omega_{ac}$.
Substituting (46) and (48) in (43) and neglecting second-order terms, we obtain the following difference-differential equation derived by Raman and Nath [31]

$$\frac{dE_m(z,t)}{dz} + \frac{\xi}{2L}(E_{m+1} - E_{m-1}) + j\frac{mk_{ac}}{\cos(\vartheta_o)}[\sin(\vartheta_0) - m\sin(\vartheta_B)]E_m = 0 \tag{52}$$

where

$$\xi = -\frac{k_f \Delta n L}{\cos(\vartheta_o)} \tag{53}$$

is a parameter related to the acoustic pressure and $2\sin\vartheta_B = \frac{k_{ac}}{k_{op}}$ (Snell's law). Here k_f is the optical wave number in free space and ϑ_B is the Bragg angle in the medium. The Bragg angle definition (52) implies a momentum-conservation relation in which the frequency shift of the diffracted light beam is neglected.

Solutions of (52) are obtained using exponential Fourier transform theory and numerical methods [9, 44, 47].

An approximate solution with a boundary condition $E_0(0,t) = 1$ and $E_m(0,t) = 0$ $(n \neq 0)$ when $\omega_a << \omega_o$, hence $m\sin\vartheta_B \approx 0$, is

$$E_m(z) = \exp\left(-j\frac{1}{2}mk_{ac}z\tan\vartheta_o\right) J_m\left(\xi\frac{\sin\left(k_{ac}z\tan\frac{\vartheta_o}{2}\right)}{k_{ac}L\tan\frac{\vartheta_o}{2}}\right) \tag{54}$$

where J_m is the Bessel function of order m [46]. The normalized intensity (to the incident beam) of the m^{th} diffracted light at $z = L$ is given by

$$I_m(z)\,|_{z=L} = \left[E_m(z)E_m^*(z)\right]_{x=L} = J_m^2\left(\xi\frac{\sin(\gamma)}{\gamma}\right) \tag{55}$$

where $E_m^*(z)$ is the complex conjugate of $E_m(z)$ and
$\gamma = k_{ac}L\tan\frac{\vartheta_o}{2} \approx Q\frac{k_{op}}{k_{ac}}\frac{\sin\theta_0}{2}$.

The last approximation is acceptable because common applications require $\theta_0 << 1$.

The parameter Q, defined by Klein and Cook [18, 19], is used in order to establish a criterion of diffraction feature. It is given by

$$Q = \frac{k_{ac}^2}{k_{op}} \frac{L}{\cos\vartheta_0} = 2k_{ac}L\frac{\sin\vartheta_B}{\sin\vartheta_0} \approx \frac{k_{ac}^2}{k_f n_0}L. \tag{56}$$

Again the last approximation is acceptable if $\theta_0 << 1$.

The Q value does not define severe limits for the working region, but in practice it is used as [19]

- Q $<\approx 0.3$ for the Raman-Nath region
- Q≈ 1 for the transition region
- Q $\geq 4\pi$ for the Bragg region

Figure 11 shows the zeroth and first order intensity levels as functions of Q at Bragg incidence with $\xi = \pi$.

In order to develop an acousto-optic device and to choose the diffraction region of operation (Raman-Nath or Bragg) one has to consider

- The optical path length L
- The optical angle of incidence ϑ_o
- The acoustic frequency f_a.

So, for a short path $\frac{L}{\lambda} < 10$ and low frequency (usually $f < 10$MHz), independent of the incidence angle, we will have Raman-Nath diffraction, and for high frequency $f > 100MHz$, long path $\frac{L}{\lambda} > 10$ and incident angle $\vartheta_o \approx \pm\vartheta_B$ we will have Bragg diffraction [11].

5.1.3 Bragg diffraction

It is found that the maximum intensity of diffracted light occurs when the incident light beam angle ϑ_o is $\vartheta_o \approx \pm\vartheta_B$. In this situation, called Bragg reflection, only the zeroth and first order diffraction are predominant while higher orders are neglected. Thus for $\vartheta_0 \approx +\vartheta_B$ (52) is reduced to

$$\frac{dE_0(z,t)}{dx} + \frac{\xi}{2L}E_1(z,t) = 0 \tag{57}$$

and

$$\frac{dE_1(z,t)}{dx} - \frac{\xi}{2L}E_0(z,t) + \frac{\zeta}{L}E_1(z,t) = 0 \tag{58}$$

where

$$\zeta = \frac{k_{ac}L}{\cos(\vartheta_o)}[\sin(\vartheta_0) - m\sin(\vartheta_B)]. \tag{59}$$

Solutions for E_0 and E_1 using $E_0(0) = 1$ and $E_1(0) = 0$ are given by [36]. The normalized intensities (to the incident light I_i) I_0 and I_1 at $x = L$ are

$$I_0 = |E_0|^2 = 1 - I_1 \tag{60}$$

$$I_1 = \left(\frac{\xi}{2\gamma'}\right)^2 \sin^2 \gamma' \tag{61}$$

where

$$\gamma' = \zeta^2 + \left(\frac{\xi}{2}\right)^2 . \tag{62}$$

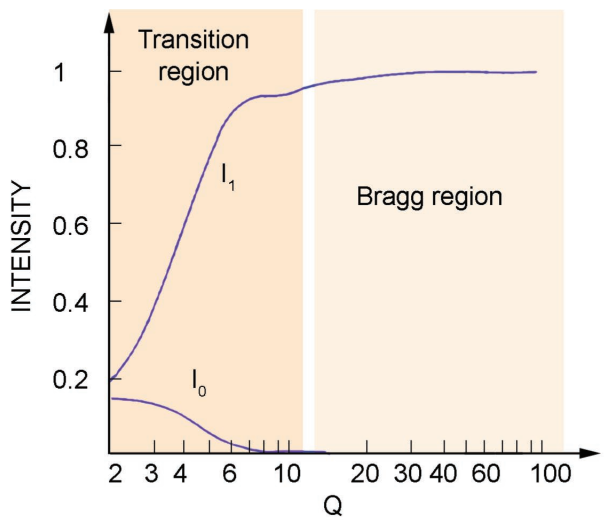

Fig. 11. Intensity of the zeroth and first order vs. Q at Bragg incidence $\xi = \pi$.

If $\vartheta_0 = +\vartheta_B$ and hence $\zeta = 0$ then (61) is reduced to

$$I_1 = \sin^2\left(\frac{\xi}{2}\right) \quad and \quad I_0 = \cos^2\left(\frac{\xi}{2}\right) \tag{63}$$

Furthermore if ξ is small then $I_1 = \left(\frac{\xi}{2\zeta}\right)^2 \sin^2 \zeta$.

5.1.4 Diffraction efficiency

In order to relate the intensity I_1 of the refracted light beam to the power P_a $[W]$ and the figure of merit M we introduce the acoustic intensity I_{ac} $[Wm^{-2}]$ given by

$$I_{ac} = \frac{1}{2}\rho\nu^3 SS^*. \tag{64}$$

Thus

$$P_{as} = I_{ac}HL = \frac{1}{2}\rho\nu_{ac}^3 SS^* HL \tag{65}$$

where ρ is the density, ν is the acoustic velocity, H is the thickness of the acoustic beam, and S^* is the complex conjugate of strain S. Here the suffix notation is omitted for simplicity.
Using (32), the variation of refractive index can be written as

$$\Delta n = -\frac{1}{2}{n_0}^3 pS = -\frac{1}{2}n_0^3 p\sqrt{\frac{2P_{ac}}{\rho\nu_{ac}^3 HL}}. \tag{66}$$

Substituting (66) in (53)

$$\xi = \frac{k_f \frac{1}{2}\frac{n_0^3 p}{\sqrt{\rho\nu_{ac}^3}}\sqrt{\frac{2P_{ac}L}{H}}}{\cos(\vartheta_o)}. \tag{67}$$

Thus the normalized intensity of the first order diffracted light at the Bragg incidence is (using 63)

$$I_1 = \sin^2\left(\frac{\pi}{\lambda_{op}\cos\vartheta_B}\sqrt{\frac{1}{2}M_2 P_{ac}\frac{L}{H}}\right) \tag{68}$$

where

$$M_2 = \frac{n^6 p^2}{\rho\nu_{ac}^3}. \tag{69}$$

The efficiency η is given by the ratio of the intensity of the diffracted light I_1 over the incident beam I_{inc}

$$\eta = \frac{I_1}{I_{inc}} = \sin^2\left(\frac{\pi}{\lambda_{op}}\sqrt{\frac{1}{2}M_2 P_{ac}\frac{L}{H}}\right). \tag{70}$$

Using the Taylor approximation,

$$\eta \approx \frac{\pi^2}{2\lambda_{op}^2}M_2 P_{ac}\frac{L}{H}. \tag{71}$$

So the efficiency of the diffraction (or deflection) is proportional to the acoustic power P_{ac}, the material figure of merit M_2 and the geometric factors L/H while it is inversely proportional to the square of the optical wavelength. From (71) a good acousto-optic material should have a high figure of merit in addition to good optical and acoustical characteristics such as low attenuation.

The figure of merit M_2 is not the only one, but others have been defined and used according to the application. The most common figures of merit are [5]

$$M_1 = \frac{n^7 p^2}{\rho \nu}$$

$$M_2 = \frac{n^6 p^2}{\rho \nu^3}$$

$$M_3 = \frac{n^6 p^2}{\rho \nu^2}$$

$$M_3 = \frac{n^8 p^2}{\rho \nu^{-1}}$$

in which n is the optical index of refraction, p the appropriate component of the photoelastic tensor, ρ the mass density, and ν the acoustic phase velocity.

It is common practice to use M_2 as a reference and to define M_1, M_3 and M_4 in relation to M_2, n and ν.

In fact $M_1 = M_2 n \nu^2$. It is used to optimize the efficiency bandwidth $\Delta f \propto n\nu^2$ [13]. Thus, the efficiency can be written as

$$\eta \approx 9 M_1 \frac{P_{ac}}{\lambda_{op}^3 f_{op} \Delta f H}. \tag{72}$$

M_2 is used when the diffraction efficiency is directly related to the acoustic power P_{ac} and the medium geometry L and H

$$\eta \approx \frac{\pi^2}{2} M_2 \frac{P_{ac} L}{\lambda_{op}^2 H}. \tag{73}$$

$M_3 = M_2 n \nu$ is used to design a reflector where the thickness H is as large as the optical beam size [8], and hence the relative diffraction efficiency will be

$$\eta \approx 9 M_3 \frac{P_{ac}}{\lambda_{op}^3 f_{op}}. \tag{74}$$

$M_4 = M_2 \left(n\nu^2\right)^2$ is applicable in the design of wideband deflectors or modulators where power density is the limiting factor. Thus, the efficiency will be given by

$$\eta \approx \frac{16 M_4}{\lambda_{op}^4 f_{op}^2 \Delta f^2} \frac{P_{ac}}{LH}. \tag{75}$$

5.2 Acousto-optic devices applications

Acousto-optic devices have long been used in a variety of laser intracavity applications. These applications can be divided into two categories: zeroth beam order applications and diffracted beam applications. Diffracted beam applications are the most common (such as modulator, deflector, tunable filter, frequency shifter) while one of the zeroth order beam applications is A-O Q-switching.

5.2.1 Modulator

The acousto-optic interaction is also used to modulate light both in amplitude and in frequency. Usually this type of device operates in the Bragg region where only one diffracted order is predominant. For proper modulator operation, the divergence of the optical beam ϕ_{op} should be approximately equal to that of the acoustic beam ϕ_{ac} [5].

For a Gaussian beam the divergence can be written as

$$\phi_{op} = \frac{4\lambda_{op}}{\pi n d} \tag{76}$$

and for an acoustic wave generated by a flat transducer of width L'

$$\phi_{ac} = \frac{\lambda_{ac}}{L'}. \tag{77}$$

Thus the divergence ratio is given by

$$a = \frac{\phi_{op}}{\phi_{ac}}. \tag{78}$$

At low values of a the maximum modulation frequency f_m approaches its limit

$$f_m \approx \frac{0.75}{\tau} \tag{79}$$

where $\tau = \frac{d}{\nu_{ac}}$ is the acoustical transient time across the optical beam.

The maximum product frequency bandwidth – peak intensity is given for a values between 1.5 and 2. That corresponds to

$$f_m \approx \frac{0.65}{\tau}. \tag{80}$$

In general, to characterize the modulator the rise time τ_R is used that is proportional to the acoustic traveling time τ through the laser beam. It is given by

$$\tau_R = \beta\tau \tag{81}$$

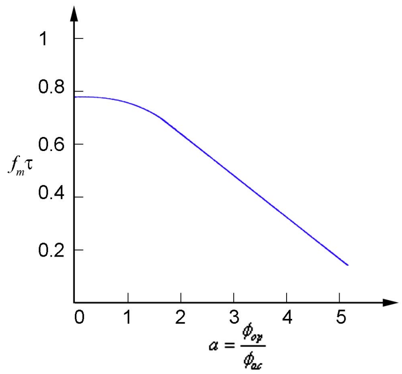

(a) Product bandwidth modulation vs. a.

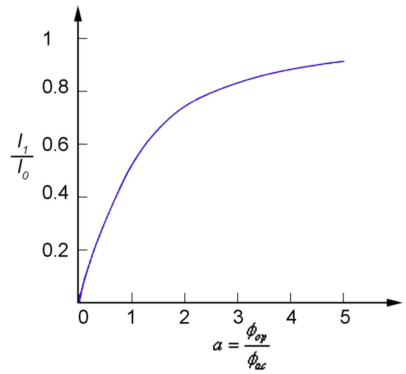

(b) Normalized maximum peak diffracted light vs. a.

Fig. 12.

where β is a constant depending on the laser beam profile. For example, for the TEM_{00} beam it is equal to 0.66.

Another requirement for the modulator device is that the diffracted and the undiffracted beam must be well separated. This implies that the Bragg angle ϑ_B should be at least equal to the optical divergence ϕ_{op}

$$\vartheta_B = \arcsin\left(\frac{\lambda_{op}}{2\lambda_{ac}}\right) \approx \frac{\lambda_{op}}{2\lambda_{ac}} = \frac{\lambda_{op} f_{ac}}{2\nu_{ac}} = \phi_{op} = \frac{4\lambda_{op}}{\pi d}, \tag{82}$$

hence the minimum center frequency is

$$f_{ac,\min} = \frac{8}{\pi\tau}. \tag{83}$$

Combining (83) and (80) we find the relation between center frequency and modulation bandwidth

$$f_{ac,\min} \approx 4 f_m. \tag{84}$$

The acousto-optic modulator has a nonlinear transfer function MTF (figure 13(b)) defined by

$$MTF = \exp\left(-\left(\frac{f_m}{1.2 f_0}\right)^2\right) \qquad f_0 = \frac{0.35}{\tau_R}. \tag{85}$$

In order to measure the separation level between the light intensity of the zeroth order and that of the first order the contrast ratio CR [29], defined as

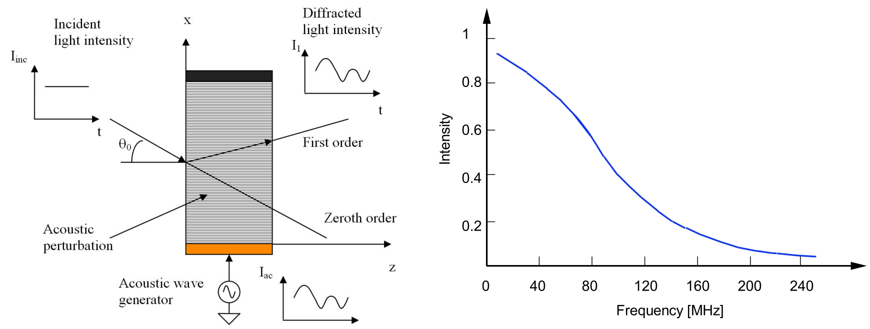

(a) Modulator: the incident light intensity is constant while the acoustical signal is variable in frequency and intensity.

(b) Different modulator transfer function according to the central freq. and bw.

Fig. 13.

$$CR = \frac{I_1}{I_0}, \tag{86}$$

is used, where I_1, is the light intensity of the first-order diffracted beam and I_0 is the light leakage of the incident beam in the direction of the first-order beam when the AO modulator is not energized. The CR value is defined for both pulse modulation mode conditions (dynamic CR) and static conditions (static CR). The dynamic CR has great importance in laser communication systems in order to measure the cross talk between zeroth and first-order channels. In general the CR value is limited by crystal imperfection and by the scattered light.

As shown by (79) the time taken for the acoustic wave to travel across the diameter of the light beam limits the modulation bandwidth. So to increase the bandwidth the diameter of the light beam must be as small as possible.

Modulators are used:

- in infrared communication applications due to the existence of several materials working in that spectral region [1, 3, 48];
- as multiplexer and demultiplexer in optical pulse code modulation using low acoustic power and standing acoustic waves;
- inside a laser cavity as Q-switching, Mode Locking and cavity dumping.

5.2.2 Deflector

An acoustic-optic deflector changes the angle of the deflecting beam proportionally to the driver acoustic frequency, so that the higher the frequency, the larger the diffracted angle (figure 14). It can be used to modulate the incident beam by shifting the position of the reflected beam on the output collimator.

The angle between the undiffracted beam and first-order diffracted beam is equal to two times ϑ_B:

$$2\vartheta_B = \arcsin\left(\frac{\lambda_{op}}{2\lambda_{ac}}\right) = \arcsin\left(\frac{\lambda_{op} f_{ac}}{2\nu_{ac}}\right). \tag{87}$$

Thus the total angle of deflection $\Delta\vartheta_d$ for a frequency change Δf_{ac} is

$$\Delta\vartheta_d = \frac{\lambda_{op}}{v_a}\frac{\Delta f_{ac}}{\cos\vartheta_0} \approx \frac{\lambda_{op}}{v_a}\Delta f_{ac} \tag{88}$$

if ϑ_0 is neglected.

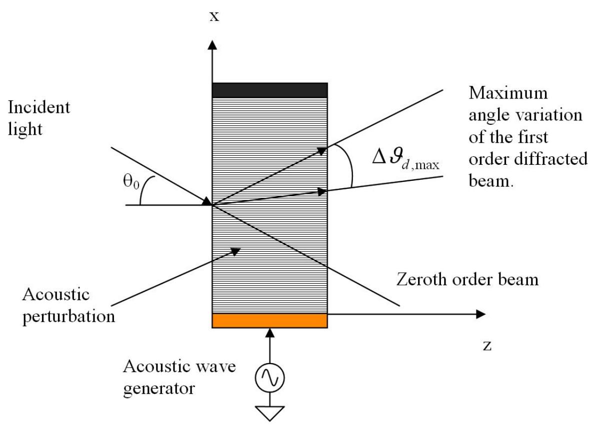

Fig. 14. Deflector working principle.

In a deflection system, there are two important performance parameters: resolution (maximum number of resolvable angular positions) and speed. The resolution N is defined as the range of deflection angles $\Delta\vartheta_{d,\max}$ divided by the angular spread of the diffracted beam ϕ_d(divergence)

$$N = \frac{\Delta\vartheta_{d,\max}}{\phi_d}. \tag{89}$$

The divergence of the diffracted beam ϕ_d will be equal to that of the incidence beam ϕ_{op} if a in (78) satisfies a<<1

$$\phi_{op} = \xi\frac{\lambda_{op}}{d}, \tag{90}$$

where ξ is a multiplication factor (near unity) that depends on the amplitude distribution of the optical beam and the criterion used for resolvability [39], and d is the diameter of the deflected beam (or of the incident beam if they are equal). Combining (89), (88) and (90)

$$N = \frac{\tau \Delta f_{ac}}{\xi} \tag{91}$$

where

$$\tau = \frac{d}{\nu_{ac} \cos \vartheta_0}. \tag{92}$$

As with the modulator, the performance of the deflector is related and limited to the transient time τ across the optical beam. But here, to the contrary, in order to increase the number of resolvable spots N, τ should be increased (directly proportional). Another limitation is due to the length L of the optical path. The spread angle in which the deflector works properly depends on whether a wide enough spectrum of plane waves is available in the radiation pattern of the transducer to satisfy the Bragg angle condition at all frequencies

$$\frac{\lambda_{ac,nom}}{L} > \frac{1}{2}\frac{\lambda}{v_{ac}}\Delta f_{ac} \tag{93}$$

or

$$L < \frac{1}{2}\frac{\lambda_{ac,nom}^2}{\lambda_{op}}\frac{f_{ac,nom}}{\Delta f_{ac}} \tag{94}$$

where $\lambda_{ac,nom}$ and $f_{ac,nom}$ are the nominal sound wavelength and frequency respectively. Equation (94) indicates that for large Δf the path length L must be decreased. This reduces the diffraction efficiency (73), and also increases the strength of additional orders by moving out of the Bragg region (56). Such difficulties may be overcome by using a phased array transducer.

Deflectors are used as:

- scanner
- switches
- spectrum analyzer
- hologram, printing, photolithography
- display driver
- cavity dumper

5.2.3 Tunable Filter

The AOTF (Acousto-optic Tunable Filter) working principle is based on the anisotropic collinear/non collinear wave interaction or isotropic collinear interaction [37]. A collinear interaction is present when the light propagates in the same direction as the acoustic wave (the wavevectors k_{ac} and k_{op} are parallel). In this case, the grating fringes are perpendicular to the direction of light propagation and the grating behaves as a pure reflection grating. On the contrary if k_{ac} and k_{op} are not parallel then a non collinear interaction will occur. In a bulk acousto-optic device the polarization of light can be rotated 90 degrees by way of the photoelastic effect produced by the acoustic strain wave. The filtered light will be separate from the unfiltered if the interaction strength L is strong enough to allow polarization to flip, for example from TE to TM. This process is resonant and narrow in spectral width because the two polarization states propagate at different velocities. Coupling can be achieved only when the phase-matching condition is met, i.e., when the sound wave momentum just compensates the TE and TM momentum mismatch [43].

The conservation of energy and momentum conditions with the phase matching condition of an acousto-optic interaction of the collinear type give the following relation [10]

$$k_o = k_e + k_{ac} or \frac{\omega_o n_0(\omega_0)}{c} = \frac{\omega_e n_e(\vartheta_e, \omega_e)}{c} + \frac{\omega_{ac}}{\nu_{ac}} \tag{95}$$

$$\boldsymbol{\omega_o} = \boldsymbol{\omega_e} + \boldsymbol{\omega_{ac}} \tag{96}$$

$$n_e(\vartheta_e, \omega_e) = \sqrt{\frac{1}{\frac{n_o^2}{\cos^2\vartheta_e} + \frac{n_e^2}{\sin^2\vartheta_e}}} \tag{97}$$

where k_e and k_o are the incident and diffracted optical momentum at the propagation angles ϑ_e and ϑ_o respectively, $n_0(\omega_0)$ and $n_e(\vartheta_e, \omega_e)$ are the refractive indexes of the ordinary and extraordinary polarizations, and w_e and w_o are the frequencies of the incident and diffracted light.

Combining (95) and (96)

$$\frac{(\omega_e \pm \omega_{ac})\, n_o}{c} = \frac{\omega_e n_e}{c} \pm \frac{\omega_{ac}}{\nu_{ac}}. \tag{98}$$

Reassembling (98) yields

$$\pm\frac{\omega_{ac}}{\nu_{ac}} \pm \frac{\omega_{ac} n_o}{c} = (n_e - n_o)\,\frac{\omega_e}{c}. \tag{99}$$

That can be approximated by neglecting the term $\frac{\omega_{ac} n_o}{c}$

$$\omega_{ac} \approx |n_e - n_o|\,\frac{\nu_{ac}}{\lambda_{op}}. \tag{100}$$

As the doped surface refractive index, such as of the waveguide surface, is more than one percent of that of the body, and hence the difference between the modal index and the substrate refractive index is less than one percent, it is possible to write (100) as [35]

$$\omega_{ac} \approx |n_{TE} - n_{TM}|\,\frac{\nu_{ac}}{\lambda_{op}}. \tag{101}$$

5.2.4 Frequency shifter

This component is used to change the frequency of the diffracted light, but also it can be a modulator or e deflector. It uses the principle of energy momentum conservation so that the scattered circular frequency is given by

$$\boldsymbol{\omega_s} = \boldsymbol{\omega_{op}} + \boldsymbol{\omega_{ac}}. \tag{102}$$

This phenomenon is called the Doppler shift. If the incident acoustic wave is introduced in the direction of the incident optical wave, the scattered optical frequency is given by (figure 15(a)).

$$f_s = f_{op} + f_{ac}. \tag{103}$$

If the incident acoustic wave is introduced in the opposite direction of the incident optical wave, the scattered optical frequency will be decreased (figure 15(b)).

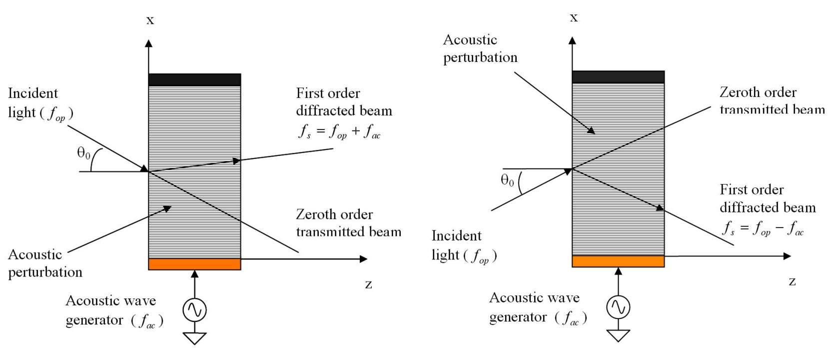

(a) Frequency up shifter. (b) Frequency down shifter.

Fig. 15. Schematic of frequency shifter.

5.2.5 Q-switch

A Q-switch is a device that, inserted into a laser cavity, allows the production of a short high energy light pulse [4, 6] (figure 16). The term Q means quality factor of a laser cavity. It is defined as the ratio of the energy stored in the laser cavity to the energy loss per cycle. Changing the cavity loss allows a change in the Q factor. When a Q-switch is turned on, the cavity loss is large enough (low Q) to inhibit laser radiation, despite continual pumping of the gain medium. When the Q-switch is turned off, the cavity loss is reduced to its minimum (high Q) and all of the energy stored in the gain medium is released in a single high-power laser pulse. By repeating this process, a sequence of laser pulses is emitted. In the Q-switching operation, the repetition rate has been limited by the time to repump the population inversion [5].

The acousto-optic Q-switch acts as a fast optical shutter that changes its polarization. The low-Q state is achieved by applying an acoustic wave to the Q-switch such that the polarization is rotated by 90 degrees. In this way, the optical feedback is lacking and the cavity can't resonate. The high-Q state is achieved by turning off the acoustic wave so that polarized laser light can move through the optical path of the cavity with minimum loss.

The Q-switch laser can be used for: materials processing (marking, cutting, welding, drilling), medical (ophthalmology and dermatology), military (sensing, range finding, target illumination) etc.

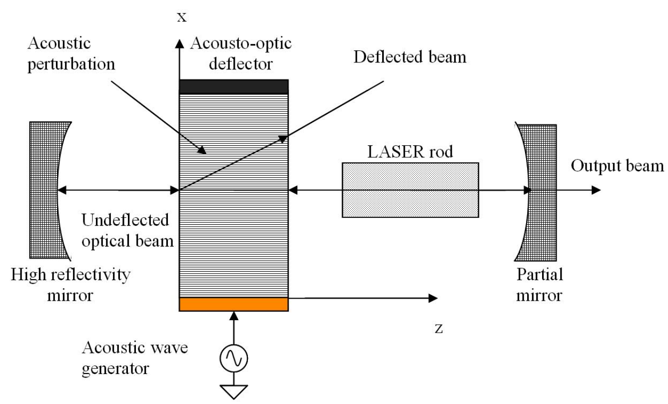

Fig. 16. Q switching LASER working principle.

5.2.6 Mode Lockers

Normally a laser can oscillate in many longitudinal modes, with frequencies that are equally separated by the intermodal spacing f_m given by [16, 40]

$$f_m = \frac{c}{2L_m}, \tag{104}$$

where L_m is the cavity length and c the light velocity. Furthermore these modes oscillate independently in free-running modes, each with its own phase with respect to the other. The mode locker (figure 17(a)) forces the phase of each mode to remain equal with respect to the other (all modes are locked in phase). In order to achieve its objective the mode locker laser uses a q-switcher inside the resonator working at frequency $f_{ac} = f_m$.

Figure 17(b) shows some parameters that characterize a mode locker laser. These parameters are:

Temporal period:

$$\tau_m = \frac{1}{f_m}, \tag{105}$$

Pulse width:

$$\tau_{pulse} = \frac{\tau_m}{N_m} \tag{106}$$

where N_m is the number of modes of oscillation,

Mean intensity:

$$I_{avg} = N_m I_0, \tag{107}$$

where I_0 is the intensity of each mode,

Peak intensity:

$$I_{peak} = (N_m)^2 I_0 = N_m I_{avg}, \tag{108}$$

Spatial period:

$$c\tau_m = 2L_m, \tag{109}$$

Pulse length:

$$c\tau_{pulse} = \frac{2L_m}{N_m}. \tag{110}$$

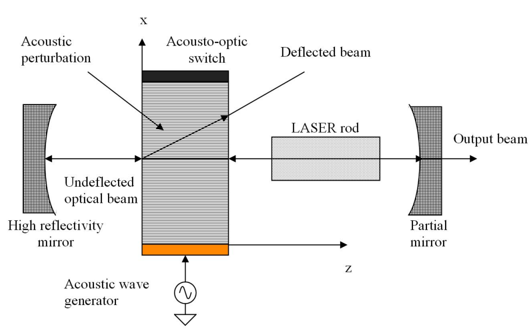

(a) Mode locker working principle.

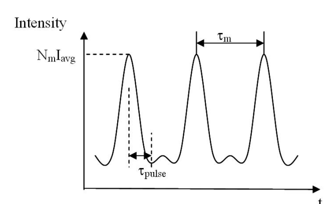

(b) Mode locker output pulses.

Fig. 17. Mode locker working principle.

In order to have stable mode locking of a laser, temperature control of the laser's environment as well as temperature control of the mode locker modulator's crystal is necessary, as any change in cavity length will result in unstable mode locking [49]. Stable mode locking of a laser also requires a very clean cavity. Any dust or contaminant inside the laser cavity will influence the laser modes.

5.2.7 Cavity dumping

The Cavity Dumping technique is used to obtain a single high-intensity pulse. An acousto-optic device placed into the laser cavity allows the production of a high power pulse (figure 18). The difference with Q-switching is that here a photon, rather than a population difference, is stored in the resonator during off-times and releasing during on-times [5]. This acousto-optic device replaces one mirror in the absence of the acoustic grating, and diffracts energy out of the cavity when an acoustic wave propagates into the mirror [17, 28].

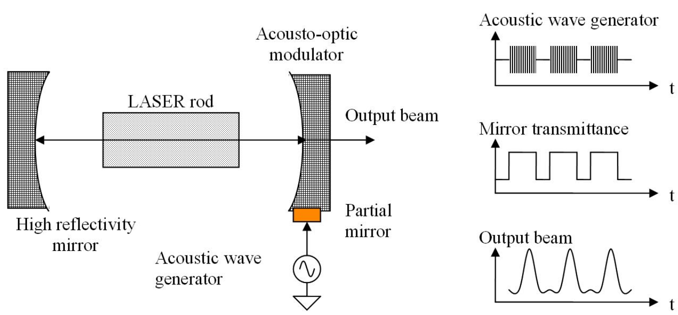

Fig. 18. Cavity dumping working principle.

6 Conclusions

This chapter gives an overview of work done over the years in the field of IR power generation and detection. In the first part we described the classical background, while in the second part acousto-optic effects are reviewed in order to give an idea of the complexity of the matter. The availability of stable IR sources in the $1 \div 14$ μm has opened the possibilities of detecting volatile compounds, even aggressive ones which manifest adsorption power, particularly in the $8 \div 14$ μm. Requirements remain for a significant miniaturization of the acousto-optic apparatus, which as of now are too expensive, large and heavy.

References

1. Abrams R. L. and Pinnow A., “Efficient Acousto-Optic Modulator at 3.39 and 10.6 Microseconds in Crystalline Germanium,” IEEE J. Quantum Electron. (Corresp.), Vol. QE-7, Mar. 1971, pp. 135-136.
2. Born M. and Wolf E., Principles of Optics, Third Edition, Pergamon Press, New York, 1965, ch. 12.
3. Chang C. and Moradian G., “Frequency Modulated Acousto-Optic modulators for 10.6 pm laser Communications, ” Electro-Optics System Design Conf., San Francisco, Nov 1974.
4. Chang Chih-Kang, Chang Jih-Yuan, Kuo Yen-Kuang - “Optical Performance of Cr:YSO Q-switched Cr:LiCAF and Cr:LiSAF Lasers.” - Proceedings of SPIE Vol. 4914 (2002) pp. 498-509.
5. Chang I.C. - Acoustooptic Devices and Applications - IEEE Transactions On Sonics And Ultrasonics vol n. 23, NO. 1, Jan. 1976.
6. Delgado M., Zalvidea Pinar D., Dez A., Prez-Milln P. and Andrs M. V. - “Q-switching of an all-fiber laser by acousto-optic modulation of a fiber Bragg grating.” - Optics Express Vol. 14, No. 3, 6 Feb2006 pp. 1106-12.
7. Dixon R. W. “Acoustic Diffraction of Light in Anisotropic Coherent Light,” Proc. ZEEE Vol. 54, Oct. 1966, pp. 1429-1437.
8. Dixon R. W. “Photoelastic Properties of Selected Materials and Their Relevance for Applications to Acoustic Light Modulators and Scanners” - J. Appl. Phys. 38 (13) pp 5149-53 (1967).
9. Dunn Derrek Butler, McNeill Mark, Jiangang Xia and Ting-Chung Poon “Three-Dimensional Analytical and Numerical Solutions for Acousto-Optic Interaction” IEEE 1997.
10. Gao Lu, Herriot Sandrine I., and Wagner Kelvin H. - “Novel Approach to RF Photonic Signal Processing Using an Ultrafast Laser Comb Modulated by Traveling-Wave Tunable Filters” - IEEE Journal Of Selected Topics In Quantum Electronics, Vol. 12, No. 2, March/April 2006.
11. Gaylord T. K. and Moharam M.G., “Analysis and Applications of Optical Diffraction by Gratings” - Proceedings Of The IEEE, Vol. 73, No. 5, May 1985.
12. Gordon E. I., “A Review of Acousto-Optical Deflection and modulation Devices,” Proc. IEEE, Vol. 54, Oct. 1966, pp.1391-1401.
13. Gordon, E.- “Figure of merit for acousto-optical deflection and modulation devices”, IEEE Journal of Quantum Electronics Vol 2, Issue 5, May 1966 pp104 - 105.
14. Henderson, Roy. Wavelength Considerations. Instituts fr Umform- und Hochleistungs. Retrieved on 2007-10-18.
15. IPAC Staff. Near, Mid and Far-Infrared. NASA ipac. Retrieved on 2007-04-04.
16. Jhon Young Min and Kong Hong Jin, “Self Q Switching of a CW Mode-Locked Nd : YLF Laser by Cavity Length Detuning” - IEEE Journal Of Quantum Electronics. VOL. 29, NO. 4, APRIL 1993 pp. 1042-45.
17. Johnson R. H., “Characteristics of acousto-optic cavity dumping in a mode-locked laser,” IEEE J. Quantum Electron., vol.QE-19, pp. 255-257, Feb. 1973.
18. Klein W . R., Cook B. D., and Mayer W. C., “Light diffraction by ultrasonic gratings,” -Acustica, vol. 15, pp. 67-74, January 1065.
19. Klein W. R. and Cook B. D., “Unified approach to ultrasonic light diffraction,” IEEE Trans. Sonics Ultrason, vol. SU-14, pp. 123-134- July 1967.

20. Korpel A, R. Atller, P. Desmares, and W. Watson, "A Televislon Display Using Acoustic Deflection and Modulation of coherent light." - Proc. IEEE vol. 54 n.10 oct. 1966.
21. Korpel A. "Acousto-Optics-A Review of Fundamentals" - Proc. Of the IEEE, VOL. 69, NO. 1, Jan. 1981.
22. Korpel A., "Acousto-optics, in Applied Solid State Science" vol. 3, R. Wolfe, Ed, Academic Press, New York (1972), ch. 2, p. 73-179.
23. Korpel, A., Acousto-Optics, Marcel-Dekker, Kea York, 1988.
24. Krishman R. S., Progress in Crystal Physics, vol. I. Sew York: Interscience, 1958.
25. Kruse P.W., McGlauchlin L.D., McQuistan R. B., "Elements of Infrared Technology", John Wiley &Sons, 1962.
26. Maldonado Theresa A. and Gaylord Thomas K. - Electrooptic effect calculations: simplified procedure for arbitrary cases - Applied Optics 15 December 1988 / Vol. 27, No. 24 pp. 5051-66.
27. Mason W P. , "Optical properties and the electro-optic and photo-elastic effects in crystals expressed in tensor form", Bell Sys. Tech. J., vol. 29, p. 161, 1950.
28. Maydan D., "Fast modulator for extraction of internal laser power," Appl. Phys., vol. 41, March 15,1970. pp. 1552-1559.
29. Men A. and Rosenberg M. Acoustooptical device with extremely high contrast ratio - Applied Optics Vol. 22, No. 6 15 March 1983 pp 873-875.
30. Miller, Principles of Infrared Technology (Van Nostrand Reinhold, 1992), and Miller and Friedman, Photonic Rules of Thumb, 2004.
31. Nath N. S. N., "The diffraction of light by high frequency sound waves :Generalized theory", vol. 4.4, pp. 222-242, 1937.
32. Nelsen D.F. and Lax M. - Theory of the Photoelastic Interaction - Physical Review B 1971 pp. 2778-2794.
33. Ngoi B. K. A., Venkatakrishnan K., Tan B., Stanley P. and Lim L. E. N. - Angular dispersion compensation for acoustooptic devices used for ultrashort-pulsed laser micromachining - 13 August 2001 / Vol. 9, No. 4 / Optics Express 2000.
34. Nye J. F. - "Physical Properties of Crystals", Sew York: Oxford, 1960.
35. Ohmachi Yoshiro and Noda Juichi -"LiNb03 TE-TM Mode Converter Using Collinear Acoustooptic Interaction" IEEE Journal Of Quantum Electronics, Vol. QE-13, No. 2, February 1977.
36. Phariseau P., "On the diffraction of light by progressive supersonic" - Indian Acad. Sci., vol. 28A, pp. 54-62, 1948.
37. Quate C. F., Wilkinson C. D. W., and 9; K. Winslow, "Interaction of Light and Microwave Sound," Proc. IEEE, Vol. 53,oct 1965 pp 1604-23.
38. Raman C. V. and Nath N. S. N., "The diffraction of light by high frequency sound waves," Proc. Indian Acad. Sci. Pt. I, vol. 2A, pp. 406-412, 1935; Pt. II, vol. 2A, pp. 413-420, 1935; Pt. III, vol. 3.4 pp. 459-465, 1936.
39. Randolph J. and Morrison J., "Modulation Transfer Characteristics of an Acousto-Optic Deflector," Apply. Optics, Vol. 10, 1971, pp. 1383-1385. "Rayleigh-Equivalent Resolution of Acousto-Optic Deflection Cells" Appl. Optics, Vol. 10, 1971, pp. 1453-4.
40. Saleh Bahaa E.A., Teich Malvin Carl - Fundamentals of Photonics - John Wiley & Sons, Inc. 1991 pp.826-827.
41. Sapriel J., Acousto-optics, John Wiley & Sons, 1979.

42. Schmid M., Weber R., Graf Thomas, Roos M. and Weber Heinz P. - Numerical Simulation and Analytical Description of Thermally Induced Birefringence in Laser Rods- IEEE Journal Of Quantum Electronics, VOL. 36, NO. 5, May 2000.
43. Smith David A., Chakravarthy Rohini S., Bao Zhuoyu, Baran Jane E., Jackel Janet L. d'Alessandro Antonio, Fritz Daniel .J., Huang S. H., Zou X. Y., Hwang S.-M., Willner Alan E. and Li Kathryn D.- "Evolution of the Acousto-Optic Wavelength Routing Switch" - Journal Of Lightwave Technology, Vol. 14, No. 6, June 1996.
44. Tarn Chen-Wen and Banerjee Partha P. - A Fourier Transform Approach to Acoustooptic Interaction of Curved, CW Ultrasonic Waves and Optical Beams with Arbitrary Profiles - proc. IEEE 1992 pp. 566-8.
45. Tsai Chen S.- Guided-Wave Acoustooptic Bragg Modulators for Wide-Band Integrated Optic Communications and Signal Processing - IEEE Transactions On Circuits And Systems, VOL. CAS-26, NO. 12, DEC 1979.
46. Uchida Naoya and Niizeki Nobukazu -Acoustooptic deflection materials and techniques - proceedings of the ieee, vol. 61, no. 8, august 1973.
47. Venzke Clark, Korpel Adrian and Mehrl David - Improved space-marching algorithm for strong acousto-optic interaction of arbitrary fields - Applied Optics / Vol. 31, No. 5 / 10 February 1992.
48. Warner A. W. and Pinnow D. A., "Miniature Acousto-Optic Modulators for Optical Communications." J. Quantum Electron.,Vol. QE-9. Dic 1973, p 1155-1157.
49. Wisoff P.J.K. and Young J. F. -"Active Mode Locking of a Microwave-Pumped XeCl Laser" IEEE Journal Of Quantum Electronics, VOL. QE-20, NO. 3, Mar 1984 pp.195-197.